The Journal of Engineering Research Vol. 5, No.1, (2008) 79-96

Comparison between Experimental and 3D Finite Element Analysis of Reinforced and Partially Pre-Stressed Concrete Solid Beams Subjected to Combined Load of Bending, Torsion and Shear

A. S. Alnuaimi

Department of Civil and Architectural Engineering, College of Engineering, PO Box 33, PC 123, Al-Khoud, Muscat, Oman

Received 8 August 2006; accepted 8 April 2007

مقارنة بين النتائج المعملية والتحليل الفراغي باستخدام العناصر المحددة لجوائز مصمته من الخرسانة المسلحة وجوائز خرسانية جزئية الاجهاد اخضعت لأحمال مجتمعة من الانحناء والالتواء و القص

علي النعيمي

الخلاصة: تعرض هذه الورقة تحليلا لا خطيا لثلاثة جوائز مصمته من الخرسانة المسلحة وجائزين من الخرسانة سابقة الاجهاد جزئيا باستخدام برنامج حاسوبي يستخدم طريقة العناصر المحددة الذي يستعمل عنصرا ثلاثي الابعاد ذا عشرين نقطة. وقد مثل سلوك الخرسانة في البرنامج باستخدام نموذج مرن لا خطي يعزى الى كوتسوفوس، بينما تم تمثيل سلوك حديد التسليح كعناصر مدفونة ذات سلوك مرن ومطاطي خالص. وقد اخذ في الحسبان خاصية الخرسانة في ابقاء مقاومة القص وخاصية مقاومة الشد بعد التشقق. كما استخدم نموذج الشقوق المشتته مع افتراض بقاء الشق في اتجاه ثابت فقط. وقد كانت ابعاد المقطع العرضي للجائز ٣٠٠×٣٠٠ مليمتر وطول الجائز ٣٨٠٠مليمتر واخضعت الى احمال مجتمعة من الانحناء والالتواء والقص. وقد تمت مقارنة النتائج المعملية بنتائج التحاليل اللاخطية. وكانت عناصر المقارنة تتضمن العلاقة بين الإزاحة والحمل، ومقدار التشوه في الحديد، وزاوية الفتل، والاحمال المسببة للانهيار، وانماط التشقق ونوع الانهيار. وقد لوحظ أن الموافقة كانت جيده بين الاحمال النهائية التي حصل عليها من التحليل اللاخطي والاحمال التي قيست في المعمل. ويستنتج من ذلك ان برنامج الحاسوب المستخدم في التحليل يمكن استخدامة بكل ثقة للتنبؤ بسلوك واحمال الانهيار للجوائز الخرسانية المسلحة والجوائز الخرسانية جزئية الاجهاد والمعرضة لاحمال مجتمعة من الانحناء والالتواء والقص.

المفردات المفتاحية: الجيزان، الجيزان المصمتة، طريقة التصميم المباشر، إنحناء، إلتواء، قص، الخرسانة المسلحة، الأجهاد.

Abstract: This paper presents a non-linear analysis of three reinforced and two partially prestressed concrete solid beams based on a 20 node isoparametric element using an in-house 3D finite element program. A non linear elastic isotropic model, proposed by Kotsovos, was used to model concrete behaviour, while steel was modelled as an embedded element exhibiting elastic-perfectly plastic response. Allowance was made for shear retention and for tension stiffening in concrete after cracking. Only in a fixed direction, smeared cracking modelling was adopted. The beams dimensions were 300x300 mm cross section, 3800 mm length and were subjected to combined bending, torsion and shear. Experimental results were compared with the non-linear predictions. The comparison was judged by load displacement relationship, steel strain, angle of twist, failure load, crack pattern and mode of failure. Good agreement was observed between the predicted ultimate load and the experimentally measured loads. It was concluded that the present program can confidently be used to predict the behaviour and failure load of reinforced and partially prestressed concrete solid beams subjected to a combined load of bending, torsion and shear.

Keywords: Beam, Solid beam, Bending, Shear, Torsion, Direct design, Concrete, Reinforced concrete, Stress analysis, Combined loading

Notation

M_d, T_d, V_d = Design bending moment, torsion and shear force respectively

L_e/L_c = Experimental to computed failure load ratio

L.F. = Load factor (percentage of applied load to design load) L.F.= $(T/T_d+M/M_d)/2$

EXP = experimentally measured values

f_{cu} = concrete cube compressive strength

Corresponding author e-mail:alnuaimi@squ.edu.om

The Journal of Engineering Research Vol. 5, No.1, (2008) 79-96

f'_c = concrete cylinder compressive strength

f'_t = concrete tensile strength

f_y = Yield stress of the longitudinal steel

f_{yv} = Yield stress of the transverse steel

f_{pu} = ultimate strength of the pre -stressing wire

τ_{shr} = Shear stress in concrete due to shear force

τ_{tor} = Shear stress due to torsion

ε_y = longitudinal steel yield strain ($\varepsilon_y = f_y/E$)

ε_{py} = prestressed wires yield strain ($\varepsilon_{py} = f_{py}/E$)

ε_{yv} = transverse steel yield strain ($\varepsilon_{yv} = f_{yv}/E$)

G = the elastic shear modulus of the un -cracked concrete

β = shear retention factor

ε_{cr} = cracking strain ($\varepsilon_{cr} = \frac{f'_t}{E_c}$)

ε_n = average of the three principal strains at any cracked point ($\varepsilon_n = \frac{\varepsilon_1 + \varepsilon_2 + \varepsilon_3}{3}$)

θ_i = Angle of twist at a section $\theta_i = (d_f+d_r)/L_h$ (See Fig. 9)

ϕ = Rate of twist $\phi = (\theta_2 - \theta_1)/a$

1. Introduction

The behaviour of solid beams when subjected to combined loading is very complex. A detailed analysis would normally require a three-dimensional finite element model.

Preston and Austin (1992) cited that "*The design and analysis of RC beams is so complex that, in general, it is impossible for engineers to consider all aspects of a problem at once*". Ojha, *et al*. (1974) have studied the behaviour of reinforced concrete rectangular beams under combined torsion, bending and shear and found a sharp reduction in the torsional stiffness compared to flexural stiffness after cracking of the beam. The reduction depends on a number of factors such as the loading combination, the strength and distribution of the steel reinforcement and the form of the cross section.

Tests conducted by Thurlimann (1979), revealed that the torsional strength of beams relies on the outer concrete shell of about 1/6 the diameter of the largest circle inscribed into the perimeter connecting the corner longitudinal bars. Mitchell and Collins (1974), described the torsional shear stress as circulating in the periphery of the section. Its intensity is distributed in a parabolic shape with the maximum stress at the outside fibre and zero at some distance from the surface. Rahal and Collins (1995) developed a three-dimensional analytical model capable of analysing rectangular sections subjected to combined loading of biaxial bending, biaxial shear, torsion and axial load. The model takes into account the shear-torsion interaction and concrete spalling. It idealizes the rectangular cross-section resisting shear and torsion as made of four transversely reinforced walls with a varying thickness and varying angle of a principal compressive strains. The vertical shear stress due to the shear force is uniformly resisted by the vertical walls and the lateral shear stress is resisted by the horizontal walls. They tested their model and concluded that the model predicts very close results to experimental behavioural and ultimate load results. Rahal (2000) developed an equation relating the ultimate torsional moment and ultimate shearing stress in the walls of the equivalent tube. The walls of the section resisting the shear stresses were idealized as a reinforced concrete membrane element subjected to pure in-plane shearing stress. MacGregor and Ghoneim (1995) stated that "*in a solid section, the shear stresses due to direct shear are assumed to be distributed uniformly across the width of the section, while the torsional shears only exist in the walls of the assumed thin-walled tube. For this reason, the direct summation of the two terms tends to be conservative and a root square summation is used*". They proposed design equations for torsional resistance in which the outer skin alone contributes to the torsional resistance of a solid beam. They claimed that the thickness of the wall resisting torsion in a solid member is on the order of one-sixth to one-quarter of the minimum width of a rectangular member. Ibell, *et al*. (1998) used an upper-bound plasticity analysis in a 2D model for the assessment of shear

The Journal of Engineering Research Vol. 5, No.1, (2008) 79-96

in reinforced concrete beams. The results from this model were compared with experimental results. It was recommended that the 2D analysis to be extended to more general 3D collapse analysis. Rabczuk and Eibl (2004), presented a model using a mesh free 2D Galerkin/ finite element approach. The concrete was modelled with particles and reinforcement with beam elements. For steel, an elastoplastic constitutive law with isotropic hardening and tension cut-off was used. The concrete was modelled via a continuum damage model, where an anisotropic tensile damage variable was used to capture the behaviour of concrete in tension. They used a displacement controlled approach for testing their model. They compared the results from their model with experimental results from one rectangular and one I-section pre-stressed beams. They concluded that a full 3D simulation would be more appropriate.

In this research a in-house 3-D finite element program was used for non-linear analysis of this computational study. The program was developed by El-Nuonu (1985) using Kotsovs' concrete model. This model was based on experimental data obtained at Imperial College London from tests on the behaviour of concrete under complex stress states (Kotsovos and Newman, 1979; and Kotsovos, 1979). The testing techniques used to obtain this data were validated by comparing them with those obtained in an international co-operative programme of research into the effect of different test methods on the behaviour of concrete. This model is capable of describing the behaviour of concrete under uniaxial, biaxial and triaxial stress conditions. It requires only the concrete cube compressive strength f_{cu} to define the behaviour of concrete under different stress states. More information about this model is given in (Kotsovos and Pavlovic, 1995).

2. Research Significance

Predictions from an in-house 3D FE program are compared with experimental results of solid reinforced and partially pre-stressed concrete beams subjected to combined load of bending, shear and torsion. The beams were designed using the direct design approach with plastic stress field for the reinforced beams and elastic stress field for the partially pre-stressed beams.

3. A 3D Finite Element Program

In the 3D program, a 150x150x150 mm isoparametric solid element with twenty node and twenty seven Gauss points was used. The concrete cylinder compressive strength $f_c^{'}$ is taken as $f'_c = 0.8 f_{cu}$ *N/mm*^{2}, the Young's modulus $E_c = 5000\sqrt{f_c^{'}}$ *N/mm*^{2}, the split cylinder tensile strength $f_t^{'} = 0.54\sqrt{f_c^{'}}$ *N/mm*^{2} and the Poisson's ratio was set at a constant value of 0.15. Before cracking or crushing, the concrete behaviour is assumed to be non-linear elastic isotropic. Crushing occurs at a point when all the three principal stresses are compressive and the state of stress is on the 'yield' surface. In the case of concrete crushing, complete loss of strength is assumed *ie*. no compression softening is allowed for. When the concrete cracks in any direction, concrete ceases to be isotropic and crushing can occur if the minimum principal strain (compressive) reaches a value taken as equal to 0.003. After cracking, smeared crack approach with simple tension stiffening and shear retention equations are employed to represent the post cracking behaviour of concrete (Fig. 1). Cracks are assumed to be orthogonal and once formed remain in their direction. The stress-strain relationship in tension was assumed to be linear up to $f_t^{'}$ and immediately after cracking the tensile stress f_t is reduced to 0.8 $f_t^{'}$. Thereafter, f_t decreases linearly with strain and is zero at the maximum strain of 0.003 which roughly corresponds to yield strain of steel of 0.0025. Transfer of shear stresses across cracks is modelled by means of the 'shear retention' factor β which defines the shear modulus of cracked concrete as $\hat{a}G$, where G is the elastic shear modulus of the un-cracked concrete. The shear retention factor $\hat{a} = 1.0$ if $\varepsilon_n \le \varepsilon_{cr}$ and $\hat{a} = 0.25\ \varepsilon_{cr}/\varepsilon_n$ if $\varepsilon_n > \varepsilon_{cr}$, where ε_{cr} = cracking strain ($\varepsilon_{cr} = \frac{f_t^{'}}{E_c}$) and ε_n = average of the three principal strains at any cracked point ($\varepsilon_n = \frac{\varepsilon_1 + \varepsilon_2 + \varepsilon_3}{3}$). The reinforcement is modelled as one dimensional element embedded in the solid concrete elements. Elastic-plastic stress-strain behaviour without strain hardening was used in this research. Only uniaxial resistance is considered with no provision for kinking or dowel action of bars. In the cells were the pre-stressing wires are present the pre-stressing wires are assumed to act as unstressed steel with a yield stress equal to the difference between the yield stress f_{py} and the stress at service f_{pe} (Fig. 2).

A standard incremental-iterative procedure was adopted for solution. The load increments were equal to 10% of the design load for the first two increments and 5% for the remaining increments. The maximum number of increments was 50 and the maximum number of iterations in each increment was 200. The convergence being deemed satisfactory if the ratio of the square roots of the sum of the squares of the residual forces to that of the applied loads did not exceed 5%.

The stresses in the cross-section nearest to mid-span were analysed. The stress distribution at the last converged increment was used for the analysis. In deciding on the predicted mode of failure, the load-deflection relationship, steel strain and ultimate load were taken into consideration. The program was extensively used by Bhatt and Lim (1999)(a,b) for the analysis of slabs, internal column-flat slab junctions and punching shear failure of flat slabs Lim and Bhatt (1998). Good agreement between predicted and experimental results was found.

The Journal of Engineering Research Vol. 5, No.1, (2008) 79-96

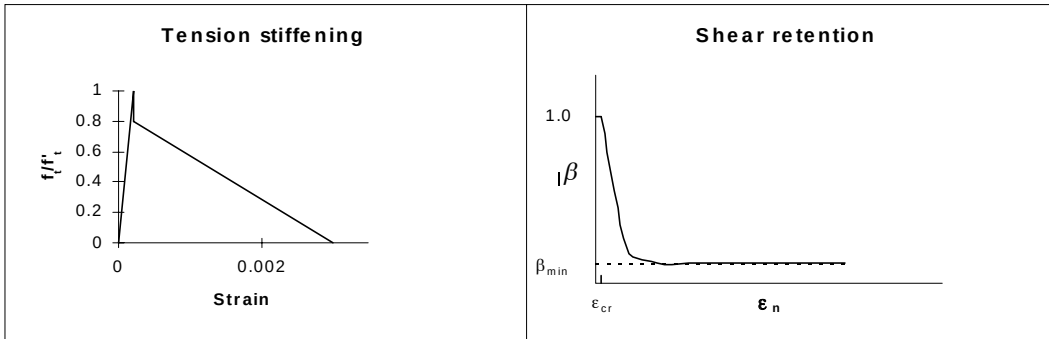

Figure 1. Tension stiffening and shear retention curves

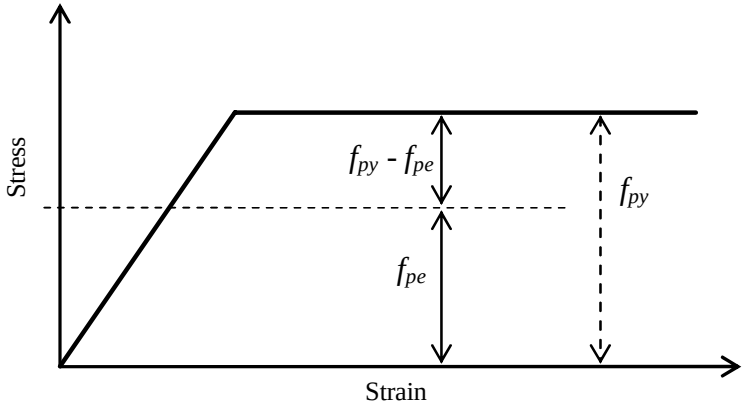

Figure 2. Transfer and service stresses in a pre-stressing wire

4. Tested Beams

Three reinforced and two partially pre-stressed concrete beams were analysed. The reinforced beams were tested by Alnuaimi and Bhatt (2006) while the partially prestressed beams were tested by Alnuaimi (2007). All beams were 300x300 mm cross section and 3.8 m length. They were subjected to a combined load of bending, torsion and shear (Table 1). The main variables studied were the ratio of the shear stress due to torsion to shear stress due to shear force τ_{tor}/τ_{shr} which varied between 0.69 and 3.04 and the ratio of the torsion to bending moment T_d/M_d which varied between 0.26 and 1.19.

The concrete mix consisted of cement, uncrushed 10mm gravel and sand with water/ cement ratio of 0.55. Three cubes, 100x100x100 mm, and six cylinders, 150x300 mm, for each beam were cast from the same concrete used for casting each beam. The specimen and the samples were kept under damp Hessian for about four days and then under room condition. The samples were tested on the day the beam was tested to determine the cube and cylinder compressive strengths and split cylinder tensile strength of concrete. The pre-stressing wires were tensioned using a simple arrangement of two nuts with ball bearings such that the wire could be stressed with a pair of spanners by tightening the nuts. The force in the wires was measured using a simple load cell developed for this purpose.

Table 2 shows the average yield strengths of reinforcement and compressive and tensile strengths of concrete. The concrete cube and cylinder compressive strengths shown for each beam in Table 2 are the measured average strengths of the three cubes and three cylinders respectively and the concrete tensile strength shown is the measured average strength of three cylinders tested for split test. All results were obtained from samples cured along side each beam. The concrete cube compressive strengths used were ranging between 37 N/mm^2 and 61 N/mm^2 (mostly normal strength concrete). Only high yield deformed bars, 8, 10 and 12 mm diameter for longitudinal and 8 mm diameter for transverse were used as reinforcement. The longitudinal steel yield strength f_y for each beam is the measured average of the average of three samples of each bar type and the transverse yield f_{yv} strength is the average measured strength of three samples. For pre-stressing only 5mm diameter wires with yield stress f_{py} of 1570 N/mm^2 were used. The calculated reinforcement was used in the test span (middle 1200 mm). Between the test span and the beam ends, more longitudinal and transverse steel was used to resist negative moment at the supports and to ensure failure occurred in the test span.

Figure 3 shows typical arrangement of reinforcement and Fig. 4 shows the provided reinforcement and arrangement of longitudinal bars for each beam. The solid circles in Fig. 4 represent the longitudinal bars or pre-stressing wires in which strain was measured nearest to mid-span. Strains in the stirrups nearest to mid-span on the front and rear faces were also reported.

The Journal of Engineering Research Vol. 5, No.1, (2008) 79-96

Table 1. Load combination

Beam No.	T_d	M_d	V_d	$\hat{o}_{tor}$	$\hat{o}_{shr}$	T_d/M_d	$\hat{o}_{tor} / \hat{o}_{shr}$
	kNm	kNm	kN	N/mm^2	N/mm^2	Ratio	Ratio
Reinforced beams							
BTV13	26	50.89	61.08	4.16	3.00	0.51	1.39
BTV14	13	50.89	61.08	2.08	3.00	0.26	0.69
BTV15	39	32.89	41.08	6.24	2.05	1.19	3.04
Partially pre-stressed beams							
BTV16	13	50.89	61.08	2.08	3.00	0.26	0.69
BTV17	39	32.89	41.08	6.24	2.05	1.19	3.04

Table 2. Average material properties

Beam No.	f_{cu}	f'_c	f'_t	f_y	f_{yv}	f_{py}
	N/mm^2	N/mm^2	N/mm^2	N/mm^2	N/mm^2	N/mm^2
Reinforced beams						
BTV13	40	28.5	3.45	500	500	-
BTV14	37	25.7	2.92	500	500	-
BTV15	61	38.2	4.38	500	500	-
Partially pre-stressed beams						
BTV16	52	36	3.42	500	500	1570
BTV17	53	36	3.44	500	500	1570

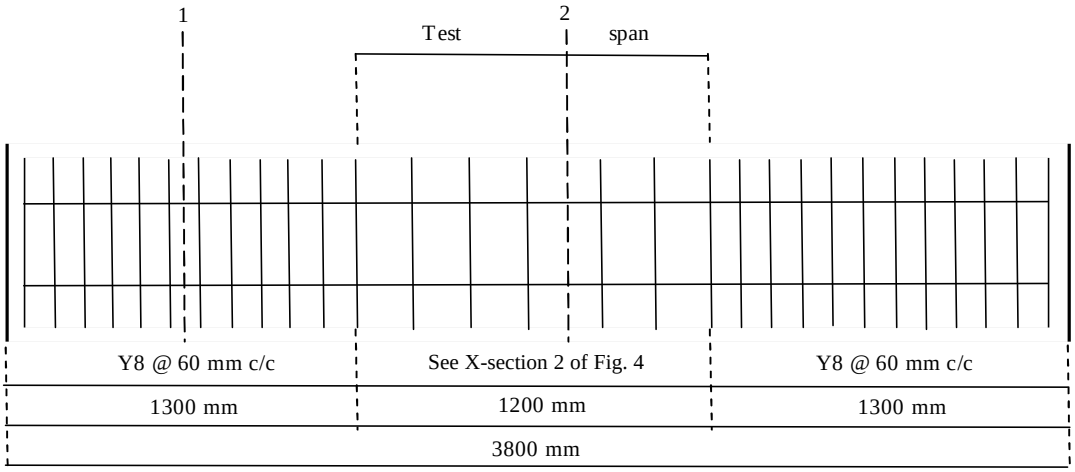

Figure 3. Typical arrangement of reinforcement

5. Test Setup and Instrumentation

Figure 5 shows typical load and support arrangement and Fig. 6 shows a testing rig with typical beam installed. The test rig is a three-dimensional frame designed to allow application of torsion, bending moment and shear force. The model was mounted on two steel stools fixed to the concrete floor at a distance of 1.8 m a part. The test span was 1.2 m long centred at mid-span. The beam was simply supported by a set of two perpendicular rollers at each support and a system of pin-and-roller at the mid-span of the top face. At the support, the lower roller allows axial displacement and the upper one allows rotation about a horizontal axis at the soffit level of the beam. The diameter of each roller was 100 mm and the length was 300 mm. The rollers were separated by 300x300x20 mm steel plates and a similar plate was put between the upper roller and the soffit of the beam. At the mid-span of the top face, a 300x100x30 mm steel plate was placed using cement plaster and the pin-and-roller system was installed between the steel plate and the load cell. The pin prevented rigid body motion and the roller allowed rotation about horizontal beam axis. Torsion was applied by means of a torsion arm fixed to each end of the beam (Fig. 7) while bending moment and shear force were a result of applied load at mid-span across the beam width at the top face.

The Journal of Engineering Research Vol. 5 No.1, (2008) 79-100

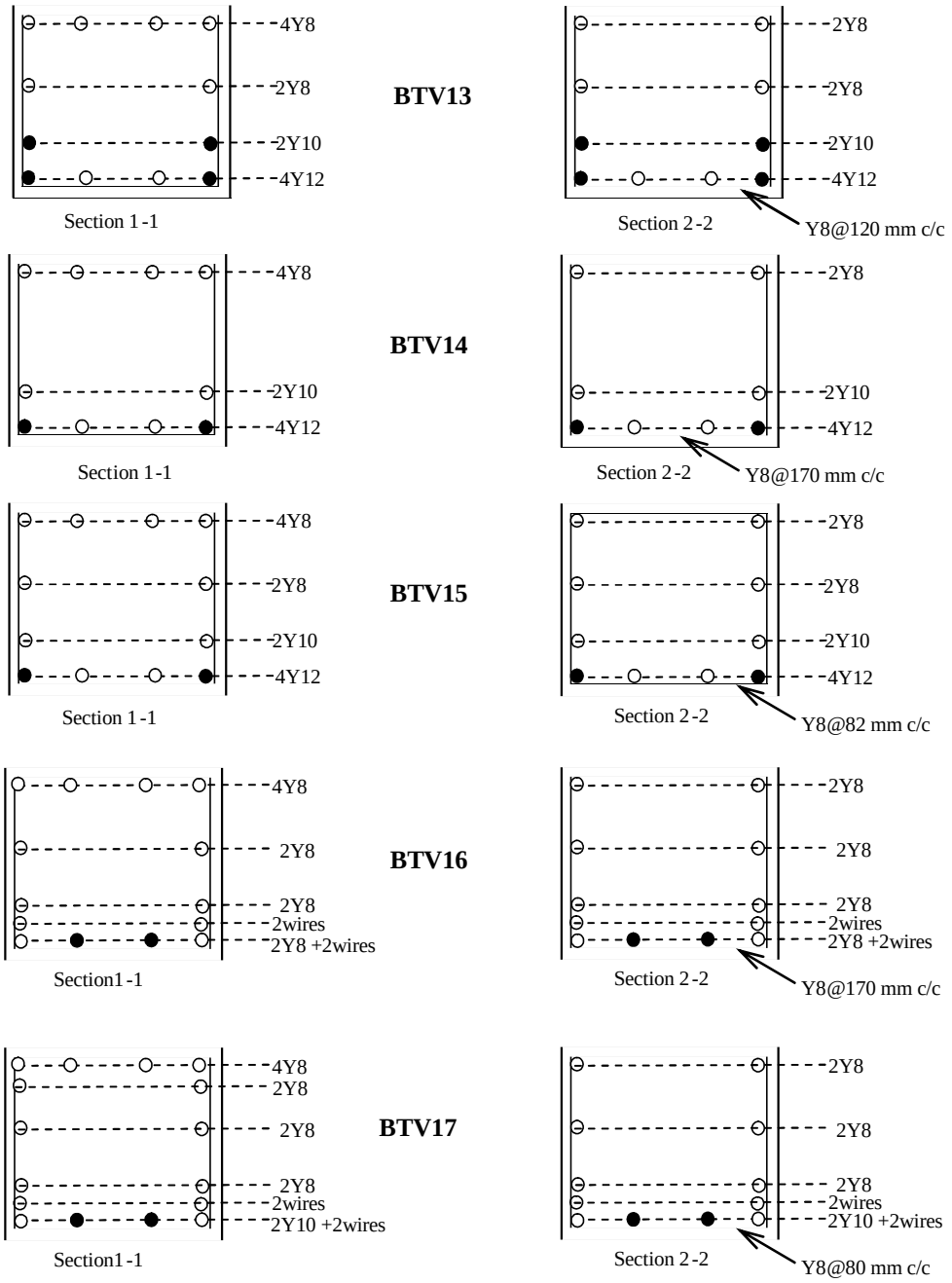

Figure 4. Provided reinforcement in the test span and outside the test span

This support and loading arrangement allowed full rotation (no torsion is resisted by the rollers) about the centre line of the beam soffit and displacement in the beam axial direction. It produced constant torsional shear stress over the entire length of the beam and maximum normal stress due to bending and shear stress due to shear force occurred near the mid-span. Torsion, bending and shear loads were applied using hydraulic pumps and load cells were used to measure the load at each jack location. The load cells were connected to a data logger for data acquisition. Linear voltage displacement transducers (LVDT) were used to measure the vertical displacement at the bottom face of the beam Fig. 8(a) while for the measurement of twist, three transducers were located on the centreline of the front and rear faces as shown in Figs. 8(b-c). Rotation at any of the vertical sections was obtained by dividing the vertical difference in displacement between directly opposite transducers by the distance between these points as shown in Fig. 9(a). Using the notations in this figure the angle of twist is equal to $(d_r+d_f)/L_h$. In the tested beams, the relative twist is the difference between the angle of twist θ_2 caused by the displacements in transducers 6 and 9 (Fig. 8) and the angle of twist θ_1 caused by the displacements in transducers 4 and 7. The rate of twist $\psi = (\theta_2 - \theta_1)/\alpha$, where α is the distance between the two sections (Fig. 9(b).

The Journal of Engineering Research Vol. 5, No.1, (2008) 79-96

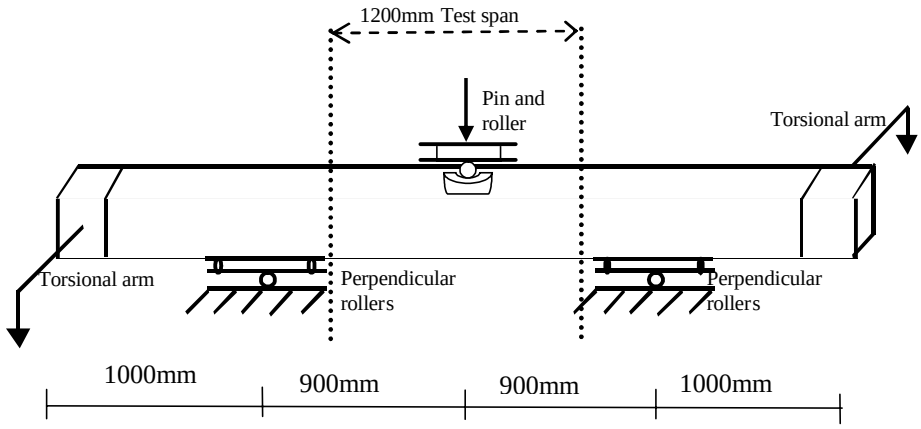

Figure 5. Typical load and support arrangement

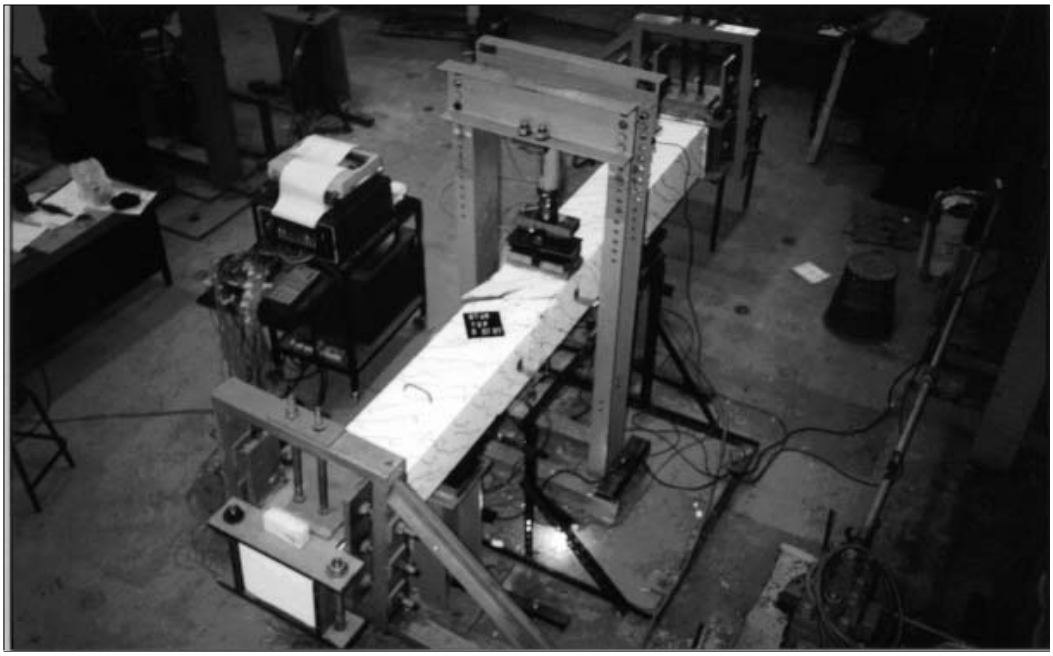

Figure 6. Test rig with a typical beam installation

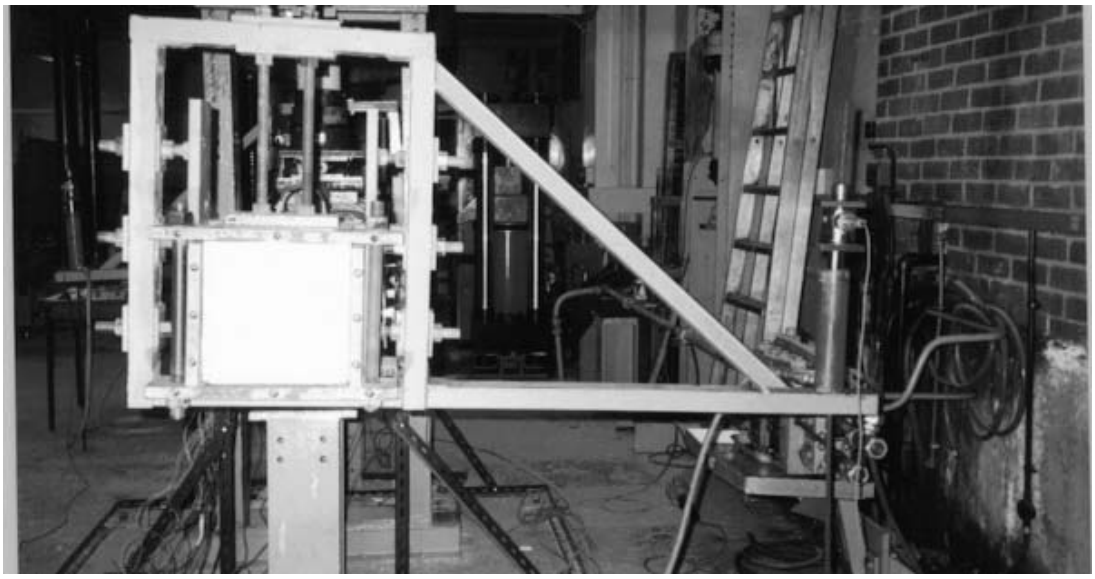

Figure 7. Torsional arm while testing

The Journal of Engineering Research Vol. 5, No.1, (2008) 79-96

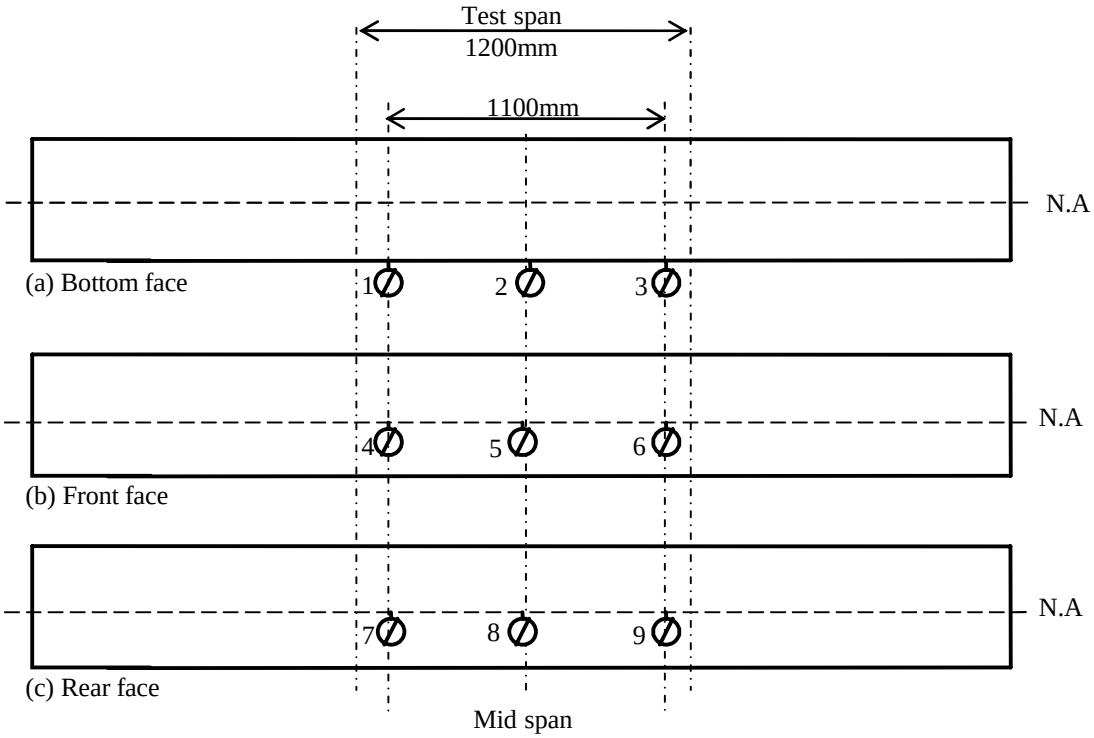

Figure 8. Locations of LVDT

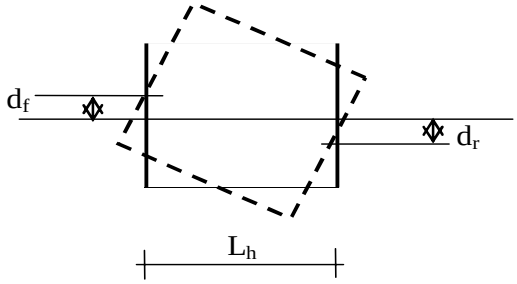

(a): Angle of twist at a section $\grave{e}_i = (d_f+d_r)/L_h$

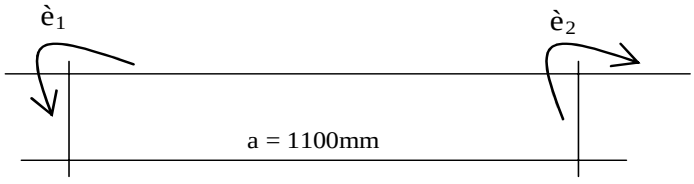

(b): Rate of twist $\text{ø} = (\grave{e}_2 - \grave{e}_1)/a$

Figure 9. Deformation of beam section due to torsion

To measure strain in the bars, a pair of strain gauges, 6mm long, was fixed on directly opposite faces of the bar and connected to a data logger. Accordingly, the axial strain recorded at each load stage was taken as the average reading of both gauges. Crack width and crack development were measured by means of a crack width measuring microscope.

For each experiment, the design load was divided into load increments. The value of each of the first three increments was 10% of the design load while for each of the rest increments it was 5% of the design load until failure. The point load applied at the mid-span and that applied at the trosional arms were exerted simultaneously until failure. The first step was to zero all load cells and record instrument readings with minimum possible loads on the model. The beam was considered to have collapsed when it could resist no more loads. This usually happened after a major crack spiralled around the beam cross-section near the mid-span dividing the beam into two parts connected by the longitudinal reinforcement.

6. Comparison between the Experimental and Computational Results

In order to obtain a finite element solution for the tested beams, the 3-D program was used for the non-linear

The Journal of Engineering Research Vol. 5, No.1, (2008) 79-96

analysis. Measured values of a concrete cube compressive strength and steel tensile strength were used. The concrete cylinder compressive strength, Young's modulus, Poisson's ratio, concrete tensile strength, shear retention and tension stiffening were used as explained in Section 3.

6.1 Load Displacement Relationship

Figure 10 shows the vertical measured and computed displacements at the centre of the bottom face of each beam. It is clear from this figure that a good agreement was achieved between experimental and computational results for beam BTV14. In the case of beams BTV13 and BTV16 the program predicted stiffer behaviour than the measured. The measured values from beams BTV15 and BTV17 were small and difficult to compare with the predicted values. With exception to the computed displacement of BTV16, measured and computed displacements of all beams with bending dominant (T_d/M_d<1) (BTV13, BTV14 and BTV16) reached the displacement limit of span/250.

The beams with torsion dominant (T_d/M_d>1) (BTV15 and BTV17) experienced measured and computed relatively smaller displacements and did not reach the span/250 limit.

6.2 Strain in the Longitudinal Steel

Figure 11 shows a good agreement between the experimental and computational results in the reinforced concrete beams for the longitudinal steel in the front face. Figure 12 shows an acceptable agreement between the measured and predicted strains in the pre-stressing wires of beams BTV16 and BTV17. In the beams with T_d/M_d<1, the longitudinal steel or prestressing wires in the front face yielded or reached yield strain while slightly less strain was recorded in the ones with T_d/M_d>1. Figure 13 shows a very good agreement in the strain ratios between the measured and predicted values of the reinforced beams in the rear face. Figure 14 shows good agreement in the case of rear face partially pre-stressed beams. In most cases, measured and predicted results show longitudinal bars or pre-stressing wires in the front faces, yielded or reached near yield strain. In the rear face, only the prestressing wires in BTV16 yielded while in the rest of the beams strain was below the yield strain.

6.3 Strain in Transverse Steel

Figure 15 shows strain ratios in the front face transverse steel; in general, a very good agreement between experimental and computational results was achieved. With exception to BTV16, the transverse steel in the front face yielded or reached near yield strain. Figure 16 shows strain ratios in the rear face transverse steel; a good agreement was achieved between the measured and predicted values in the case of beams BTV13, BTV14 and BTV17. In the case of BTV15, the program predicted larger values of strain for the same load than the measured ones. It should be noted that both measured and predicted values of strain in the rear face were negligible and the steel did not reach yield strain. This due to the fact that for practical reasons, that stirrup areas required for the front face where shear stresses are additives were used in the rear face subtractive as well. So, the beams are over reinforced in the transverse direction of the rear face.

6.4 Relative Angle of Twist

Figure 17 shows the experimental and computational relative angles of twist. These angles were calculated as explained in Section 5. It can be seen that a very good agreement has been achieved between experimental and computational results in most cases. However, in beam BTV17 the observed angle was larger than the computed one. In beams where torsion was dominant (T_d/M_d>1) the relative angle of twist was relatively larger than when the bending was dominant (T_d/M_d<1). For the same load combination, the partially prestressed beam BTV16 experienced a smaller twist than the reinforced beam BTV14. However, the difference in the case of beams BTV15 and BTV17 was negligible.

6.5 Failure Load

Column 4 of Table 3 shows a very good agreement between the measured Le and computed Lc failure loads. All beams failed near their design loads.

6.6 Crack Pattern and Mode of Failure

Both the computed and measured results showed that in the case of beams in which bending was dominant (T_d/M_d<1) almost vertical cracks started in the bottom face and at the lower half of the front and rear sides. These cracks were followed by inclined cracks in succeeding load increments until they first appear and in the top flange at about 80% of a failure load. In the beams where torsion was dominant (T_d/M_d>1), inclined cracks extended into the bottom face one increment after they were formed in the front and rear sides. In both groups, the smaller the ratio T_d/M_d, the closer is the angle of crack to vertical. Figures 18-20 show typical computed and observed crack development of the tested beams. The computed and observed cracks shown are taken at the load increment just before failure. In beams BTV13, BTV14 and BTV16 the mode of failure was mostly flexural where the beam experienced relatively large displacement and the flexural steel yielded. A small number of large cracks caused failure at the time of flexural steel yielding. Beams BTV15 and BTV17 failed by diagonal cracking due to high torsional shear stress and the failure mode was less ductile with small displacement, less longitudinal steel strain and larger transverse steel strain than the bending dominant beams. It is clear that a good agreement between the observed and computed cracks was achieved on the intensity and direction of cracks.

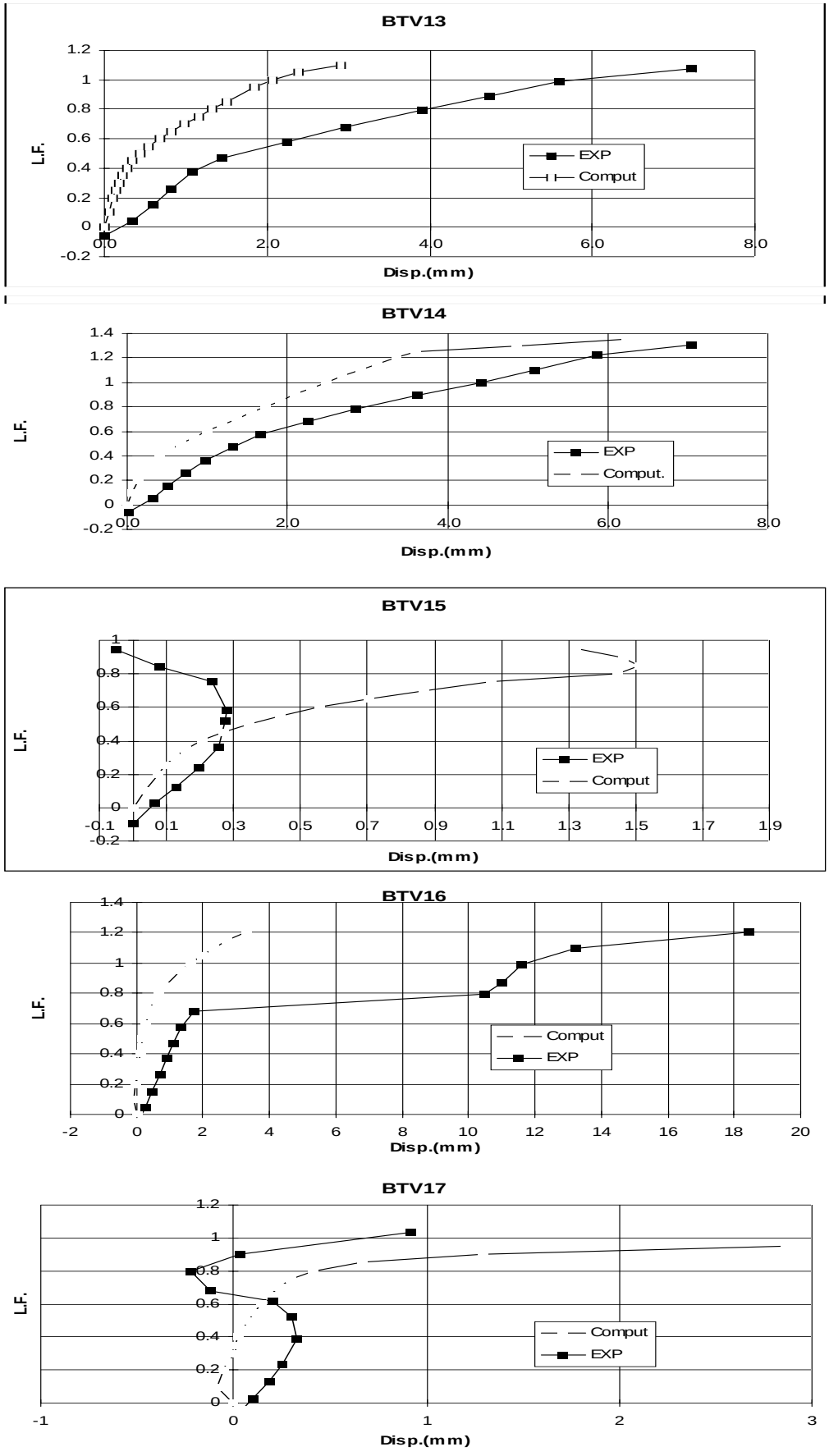

Figure 10. Vertical displacement at mid-span

The Journal of Engineering Research Vol. 5, No.1, (2008) 79-96

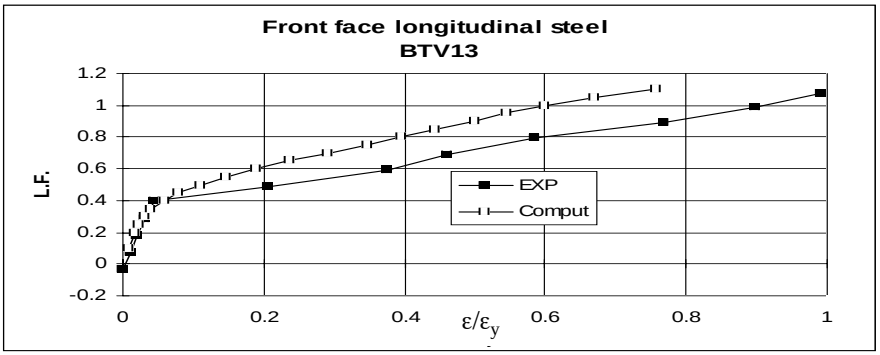

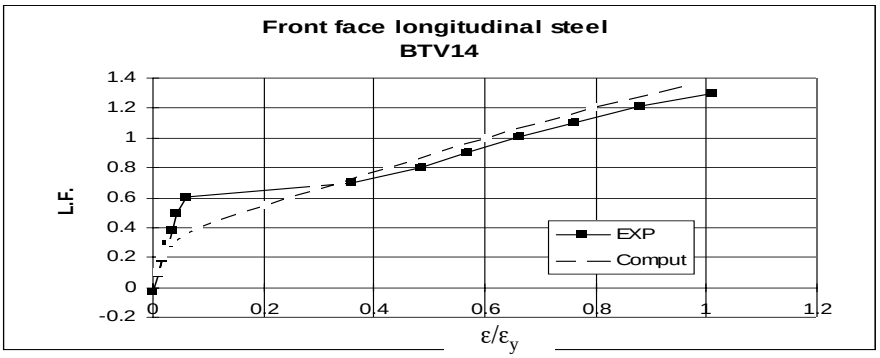

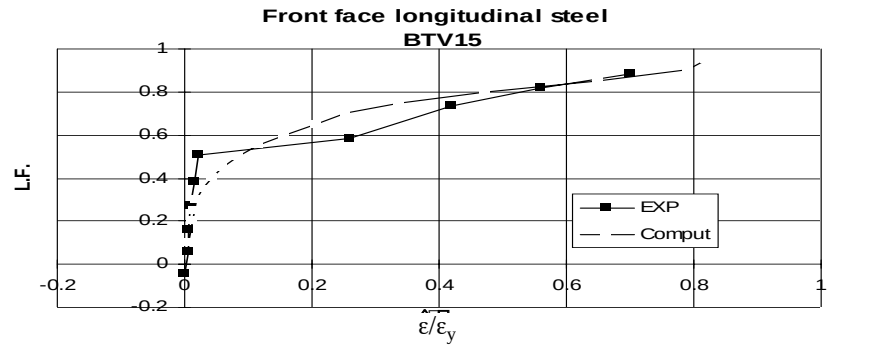

Figure 11. Strain ratios in the front face longitudinal steel

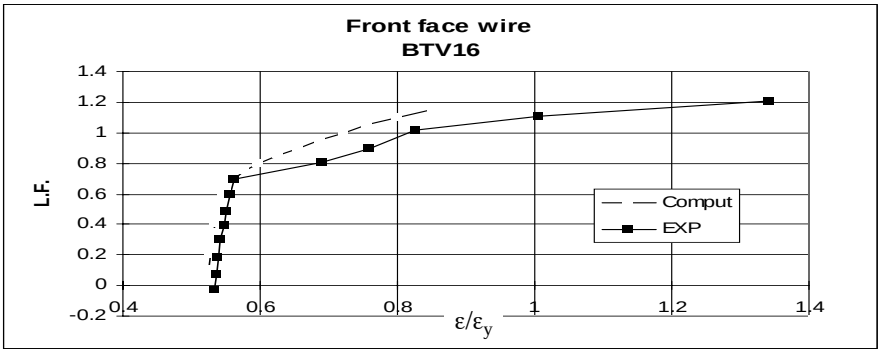

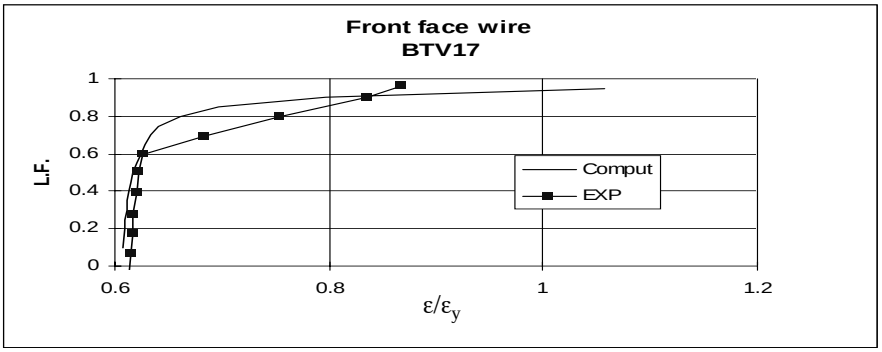

Figure 12. Strain ratios in the front face pre-stressing wires

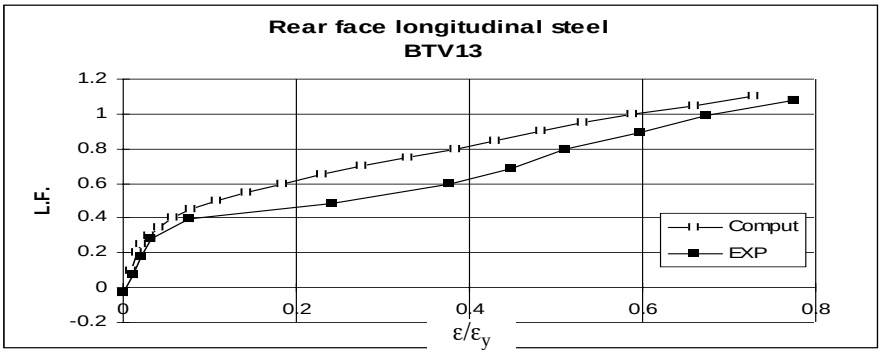

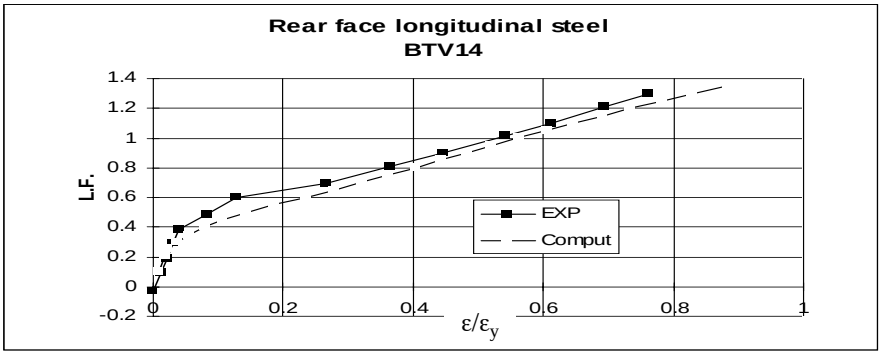

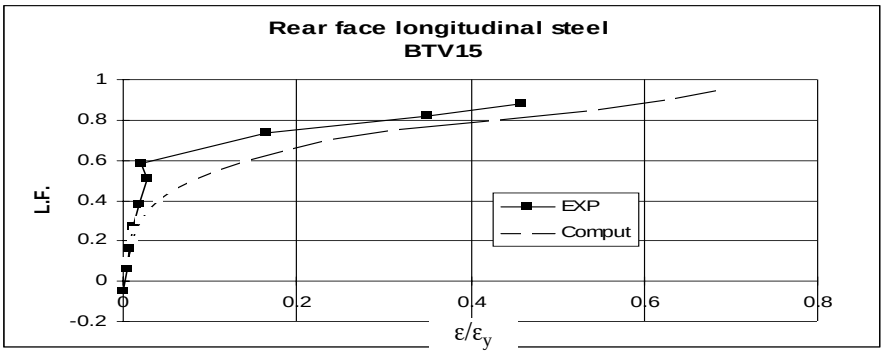

Figure 13. Strain ratios in the rear face longitudinal bars

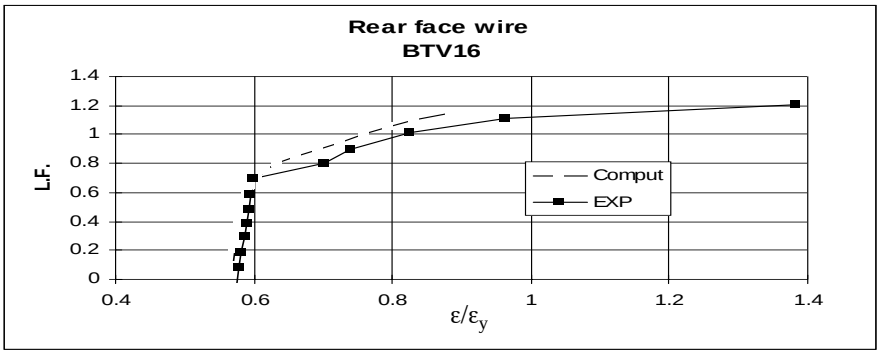

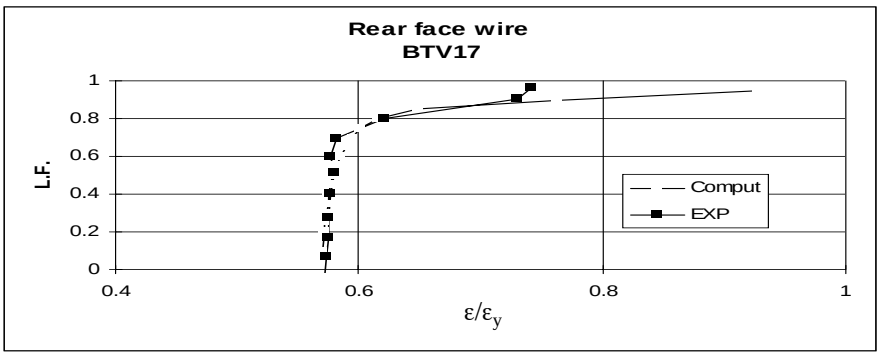

Figure 14. Strain ratios in the rear face pre-stressing wires

The Journal of Engineering Research Vol. 5, No.1, (2008) 79-96

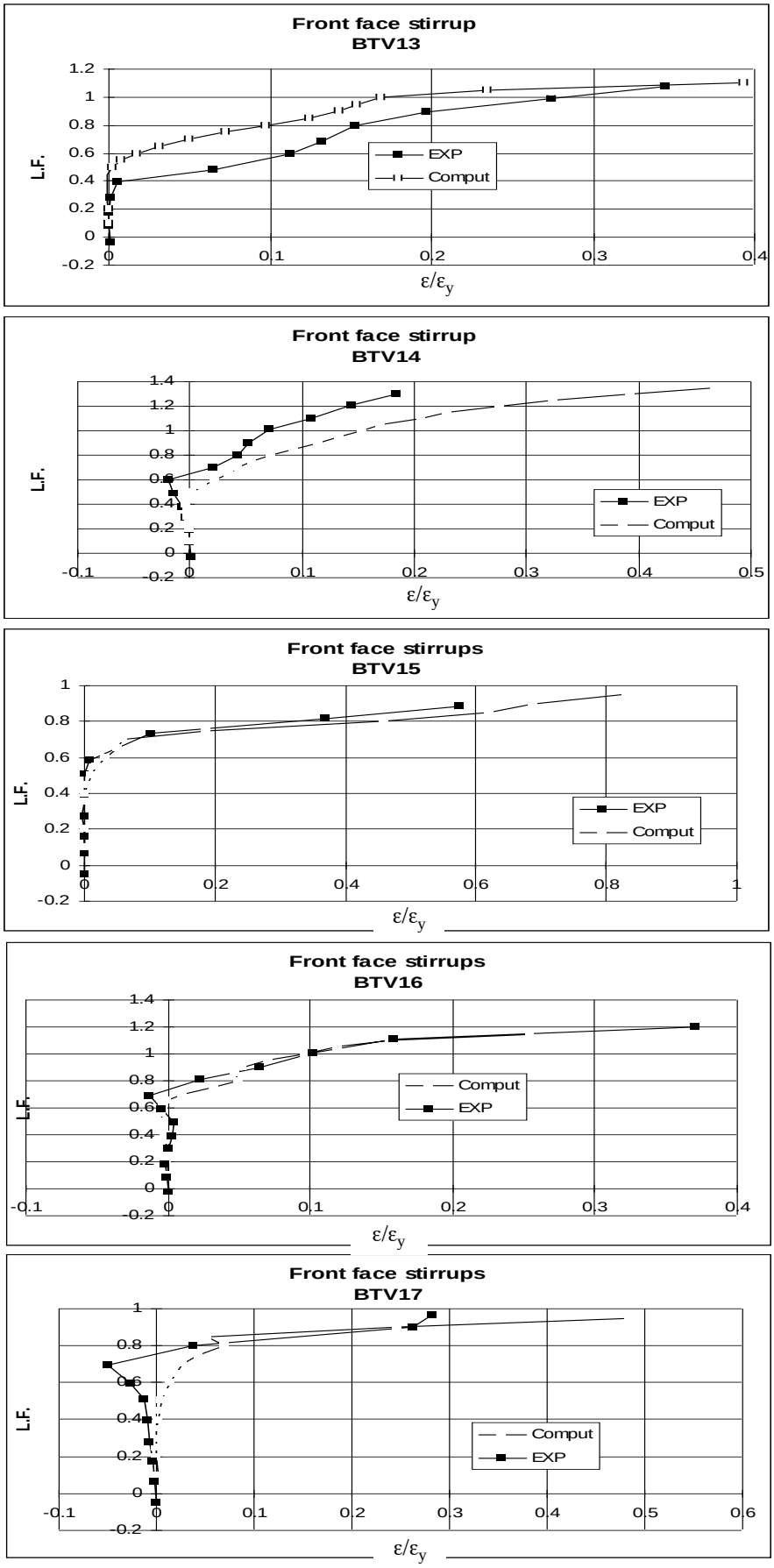

Figure 15. Strain ratios in the front face stirrups

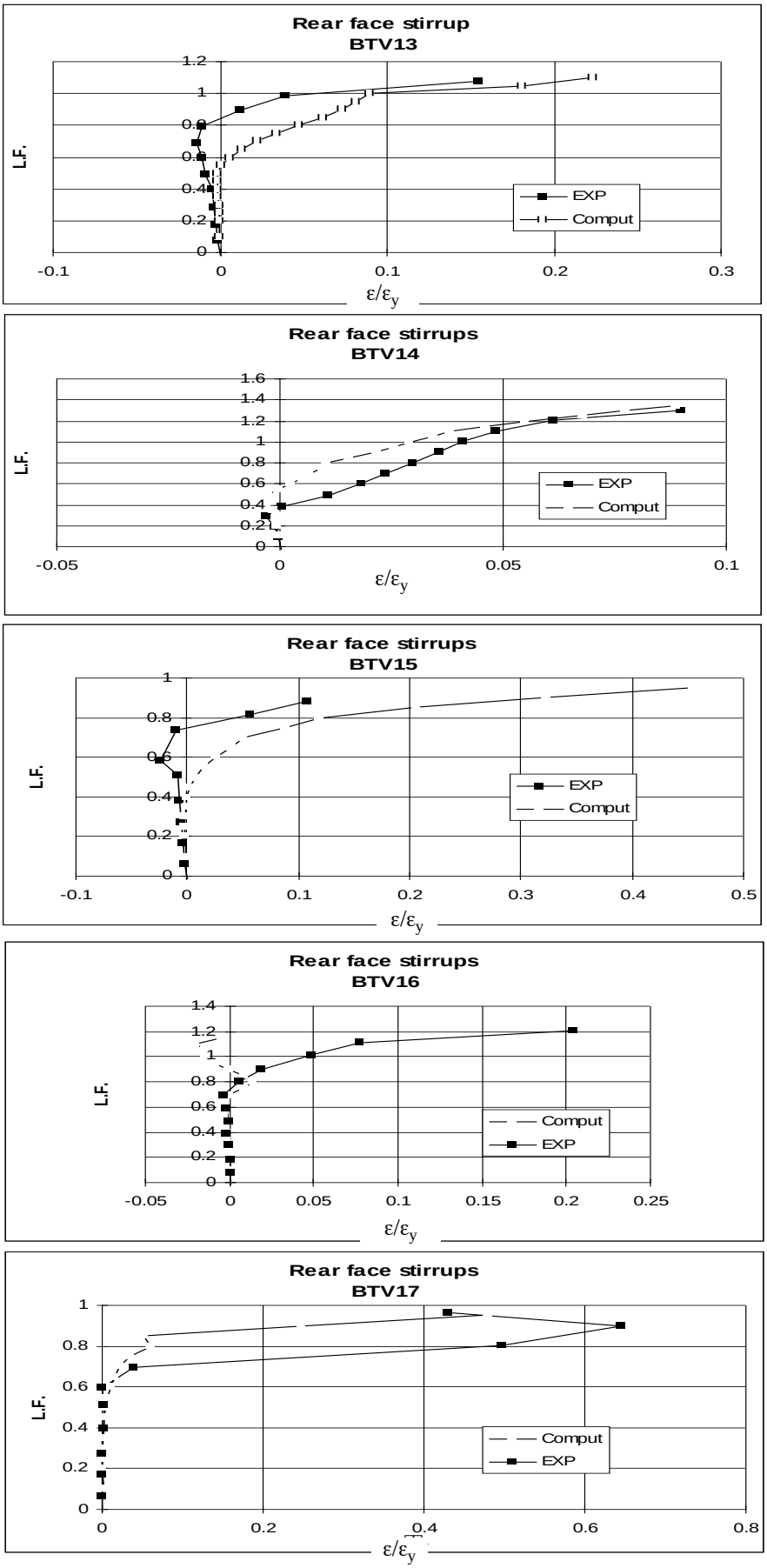

Figure 16. Strain ratios in the rear face stirrups

The Journal of Engineering Research Vol. 5, No.1, (2008) 79-96

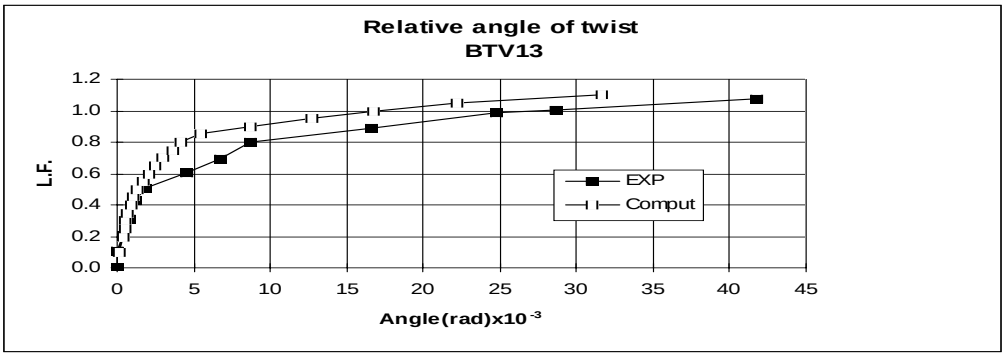

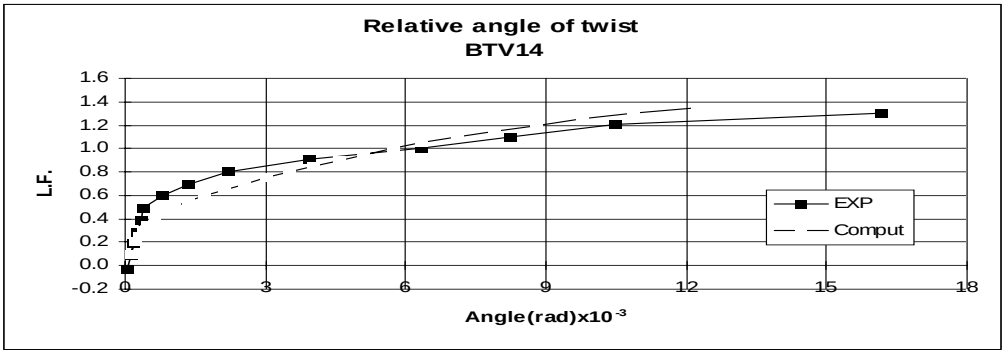

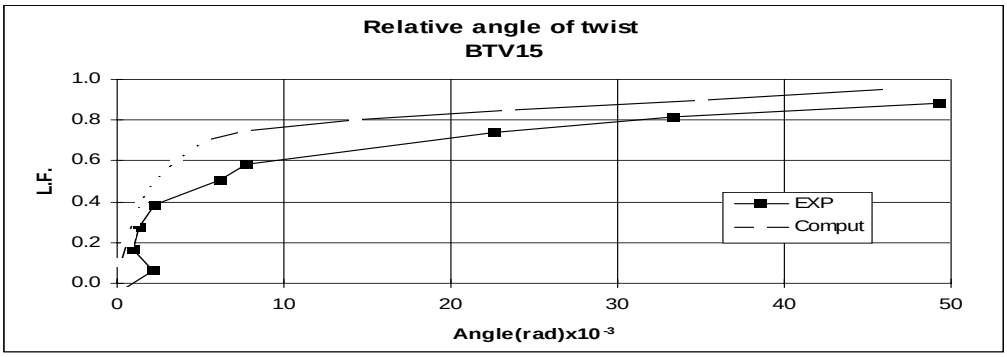

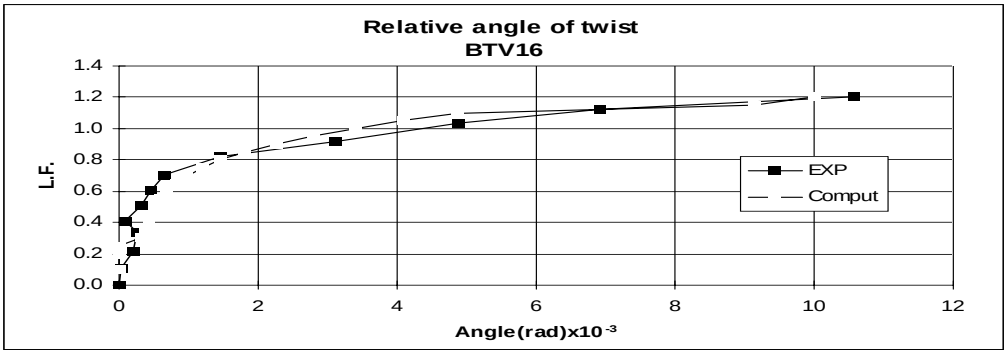

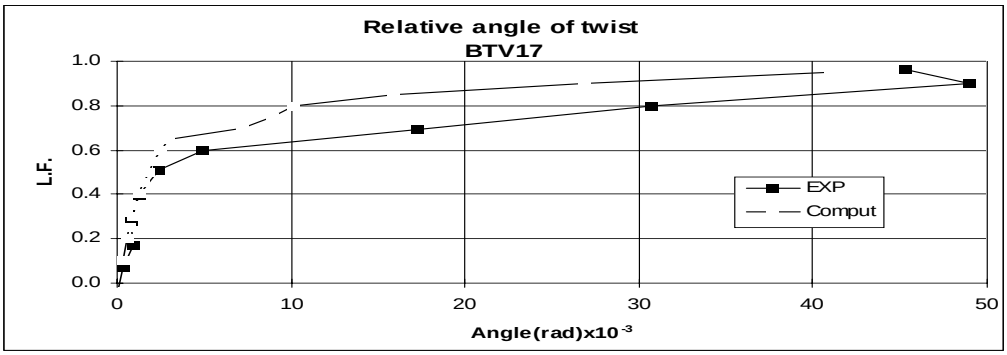

Figure 17. Relative angle of twist

The Journal of Engineering Research Vol. 5, No.1, (2008) 79-96

Table 3. ratios of measured and predicted failure loads

1 Beam No.	2 T_d/M_d Ratio	3 $\hat{o}_{tor}/\hat{o}_{shr}$ Ratio	4 L_e/L_c Ratio
	Reinforced beams		
BTV13	0.51	1.39	0.98
BTV14	0.26	0.69	0.96
BTV15	1.19	3.04	0.93
	Partially pre-stressed beams		
BTV16	0.26	0.69	1.00
BTV17	1.19	3.04	1.02
	Mean		0.98

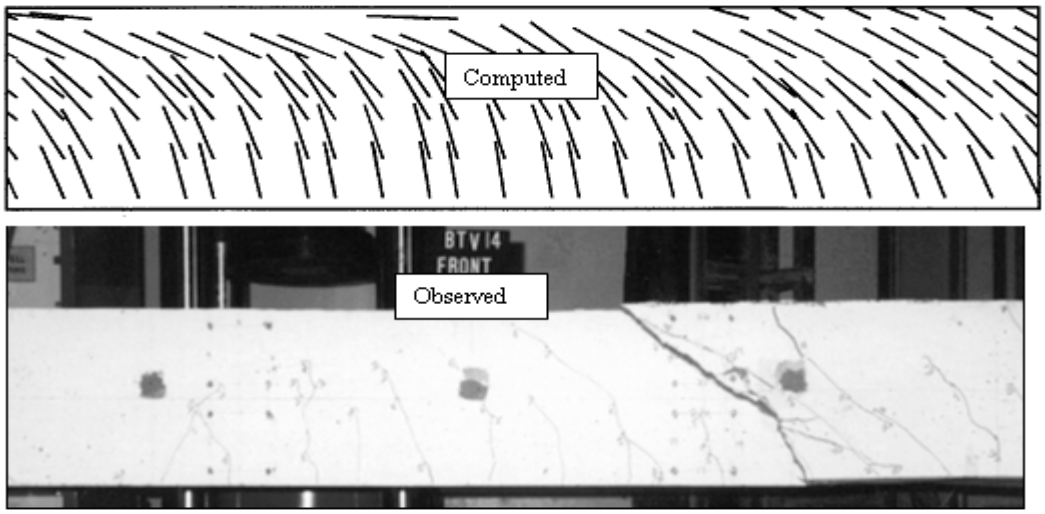

Figure 18. Computed and observed cracks near failure in the front face (BTV14)

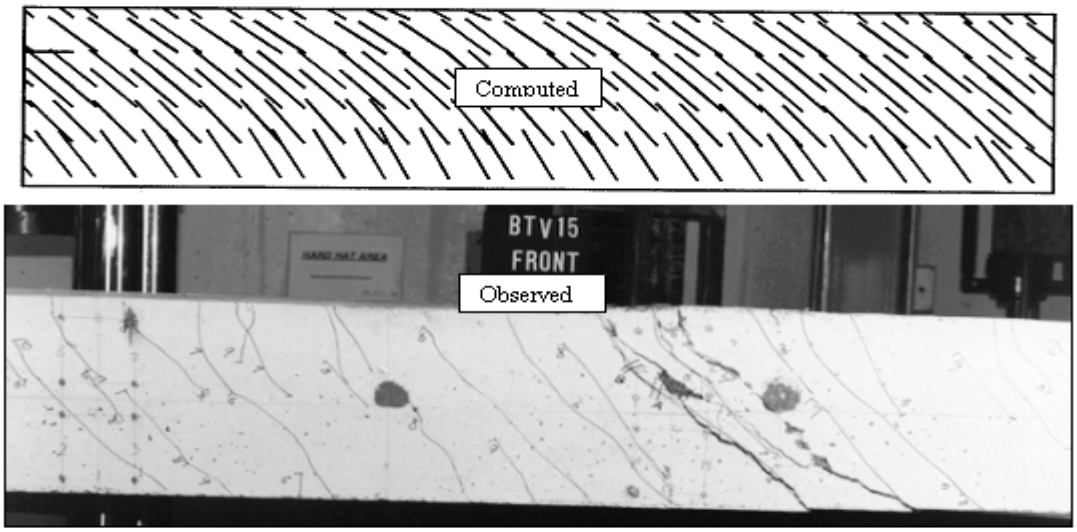

Figure 19. Computed and observed cracks near failure in the front face (BTV15)

7. Conclusions

A comparison was conducted between experimental results and an in-house 3D finite element analysis of three reinforced and two partially prestressed concrete solid beams. The beams were designed using the direct design method and subjected to different load combinations of bending, shear and torsion. The comparison was judged by load displacement relationship, steel strain, angle of twist, failure load, crack pattern and mode of failure. Very good agreements were obtained in the cases of steel strain ratios, angle of twist, failure load and mode of failure. Acceptable agreement was obtained for displacement values. Overall, it can be concluded that the predictions from the 3D finite element program was shown to be in a good agreement with the experimental results and therefore,

The Journal of Engineering Research Vol. 5, No.1, (2008) 79-96

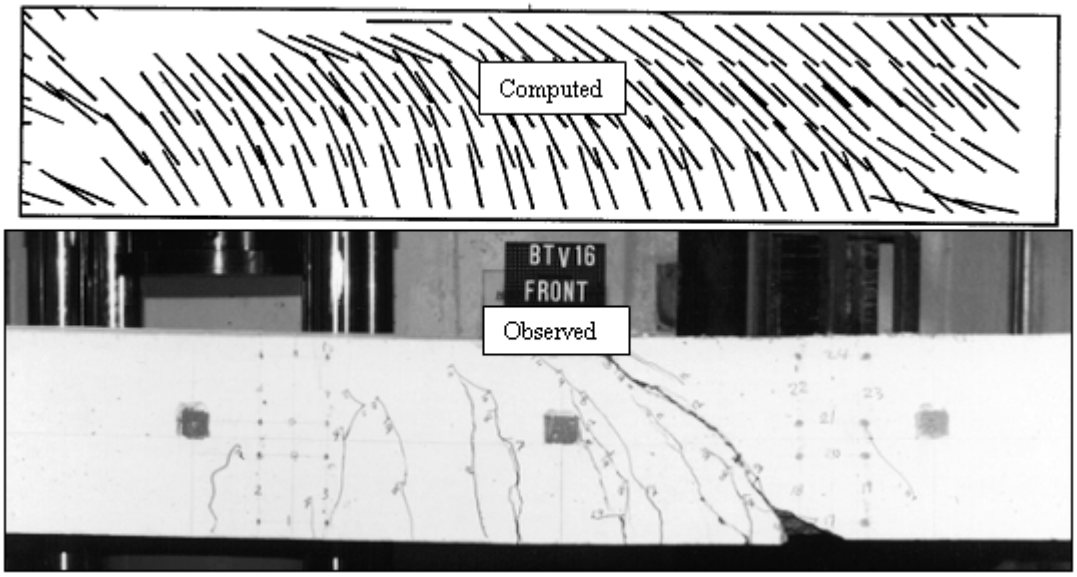

Figure 20. Computed and observed cracks near failure in the front face (BTV16)

proven to be a good tool for the prediction of beam behaviour and ultimate load of solid reinforced and partially prestressed concrete beams subjected to combined load of bending, torsion and shear. Large differences in load combinations (T_d/M_d 0.26 - 1.19 and τ_{tor}/τ_{shr} 0.69 - 3.04) did not result in large discrepancies between measured and predicted results.

References

Alnuaimi A.S. and Bhatt, P., 2006, "Design of Reinforced Concrete Solid Beams, Structures and Buildings Journal," Thomas Telford Limited, Vol. 159(4), pp. 197-216.

Alnuaimi, A.S., 2007, "Direct Design of Partially Prestressed Concrete Solid Beams Structural Engineering and Mechanics," Techno-Press Ltd, Vol. 27(6), pp. 741-771.

Bhatt, P. and Lim, B.T., 1999a, "Flat Slab-Column Junctions with Shear and Moment Transfer: A Comparison between Finite Element Predictions and Experiments," Proc. of 7th ACME Conference, University of Durham, (Ed. Bettes, P.) pp. 11 - 14.

Bhatt, P. and Lim, B.T., 1999b, "Punching Shear Capacity of Internal Column-Flat Slab Junction with In-Plane Restraint: A Comparison between Finite Element Predictions and Experiments. Developments in Analysis and Design Using Finite Element Methods," Civil-Comp Press, (Ed. B.H.V. Topping), pp. 141 - 147.

El-Nuonu, G. F. R., 1985, "Design of Shear Wall-Floor Slab Connections. Ph.D. thesis, University of Glasgow.

Ibell, T.J., Morley, C.T. and Middleton, C.R., 1998, "An Upper-bound Plastic Analysis for Shear," Magazine of Concrete Research, Vol. 50(1), pp. 67-73.

Kotsovos, M.D. and Newman, J. B., 1979, "A Mathematical Description of the Deformation Behaviour of Concrete under Complex Loading," Magazine of Concrete Research, Vol. 31(107), pp. 77-90.

Kotsovos, M.D. and Pavlovic, M.N., 1995, Structural Concrete, Finite Element Analysis for Limit-State Design," Thomas Telford Publications, 1 Heron Quey, London E14 4JD.

Kotsovos, M.D., 1979, "A Mathematical Description of the Strength Properties of Concrete under Generalized Stress," Magazine of Concrete Research, Vol. 31(108), pp. 151-158.

Lim, B.T. and Bhatt, P., 1998, "Punching Shear Failure of Flat Slabs: A Comparison between Finite Element Predictions and Experiments," Advances in Civil and Structural Engineering Computing for Practice, (Ed. B. Topping), Civil Comp-Press, pp. 163 - 173.

MacGregor, J.G. and Ghoneim, M.G., 1995, "Design for Torsion. ACI Structural Journal," Vol. 92-S20, pp. 211-218.

Mitchell, D. and Collins, M.P., 1974, "Behaviour of Structural Concrete Beams in Pure Torsion," Publication No. 74-06, Department of Civil Engineering, University of Toronto, Toronto, Ontario, Canada.

Ojha Surendra, K., 1974, "Deformation of Reinforced Concrete Rectangular Beams under Combined Torsion, Bending and Shear.," ACI Journal, Vol. 71-26, pp. 383-391.

Preston, J.I. and Austin, M.A., 1992, "Solid Modelling of RC Beams:2, Computational Environment," Journal of Computing in Civil Engineering, Vol. 6(4), pp. 404-416.

Rabczuk, T. and Eibl, J., 2004, "Numerical Analysis of Prestressed Concrete Beams using a Coupled Element Free Galerkin/Finite Approach," Int. J. of Solid and Structures, Vol. 41(3-4), pp 1061-1080.

Rahal, K.N., 2000, "Torsional Strength of Reinforced Concrete Beams," Canadian Journal of Civil Engineering, Vol. 27, pp. 445 - 453.

Rahal, K.N. and Collins, M.P., 1995, "Analysis of Sections Subjected to Combined Shear and Torsion ," A Theoretical Model. ACI Structural Journal, Vol. 92(4), pp. 459-469.

Thurlimann, B., 1979, "Torsional Strength of Reinforced and Prestressed Concrete Beams-CEB Approach," Institut fur Baustatik und konstruktion, ETH. Zurich., Vol. 92, pp 117-143. Also can be found in: American Concrete Institute, Detroit, SP59.